

## INVESTIGATION OF OPTIMISED NOTCH SHAPES FOR FLEXURAL HINGES

S. Zelenika,<sup>\*&</sup> S. Henein,<sup>#</sup> L. Myklebust<sup>\$</sup>

<sup>\*</sup> Paul Scherrer Institut, 5232 Villigen PSI, Switzerland

<sup>&</sup> University of Rijeka, Faculty of Engineering, Vukovarska 58, 51000 Rijeka, Croatia

<sup>#</sup> Centre Suisse d'Electronique et de Microtechnique, Neuchâtel, Switzerland

<sup>\$</sup> Norwegian University of Science and Technology, Trondheim, Norway

### Abstract

*High precision positioning devices based on flexural hinges are often used in 3<sup>rd</sup> generation synchrotron radiation beamlines. In this work is presented a first approach towards the optimisation of the geometry of the notches. The obtained results indicate that the optimal shape will depend on a trade-off between the possibility to increase the compliance (i.e. decrease the stress) of the notch for a given deflection on one hand and the entity of the parasitic shift accompanying the main degree of freedom of the notch on the other. The optimum will thus be chosen from the here presented guidelines based on the application the designer is confronted with.*

### 1. Introduction

In order to guarantee the stability and reproducibility of beam position, one of the most important tasks in designing 3<sup>rd</sup> generation synchrotron radiation equipment and instrumentation is the ultra-high precision positioning of optical components and other elements with resolutions, accuracies and precisions in the (sub)nanometric and micro(nano)-radian ranges [1]. In the mechanical design of the considered positioning mechanisms such requirements, especially when coupled with ultra-high vacuum and radiation compatibility needs, result very often in the usage of compliant mechanisms relying on the elastic properties of matter. Such devices are then mostly based on the employment of flexural hinges [2].

Up to recently the choice of the notch shapes for flexural hinges was determined by the available production technologies. In fact, the notches were mainly produced by conventional rotating machine tools and therefore limited to circular shapes. The availability of high-precision milling and especially Electro-Discharge Machining (EDM), as well as other micro- and meso-manufacturing technologies (e.g. deep X-ray lithography), has allowed these limitations to be overcome. The shape of the notches (Fig. 1) can therefore today be chosen based on the design requirements for the specific application.

In the design of optics manipulation mechanisms for 3<sup>rd</sup> generation synchrotron radiation beamlines, the need to achieve ever greater precision (down to an Å and nrad level) with large travels (respectively 50 mm and several degrees, i.e. needing far greater compliance) has generated thus a clear tendency to use flexural hinges of non-circular shapes [3, 4]. Other authors have recently also investigated non-circular hinge shapes with the aim of defining closed form analytical formulations of the resulting stress-strain behaviour. In [5] have hence been considered elliptical flexural hinges, whereas in [6] have been considered parabolic and hyperbolic notch shapes.

In none of the studies available in literature is, however, tackled the problem of the optimisation of the hinge shape based on the mechanical requirements of minimizing the stresses in the notches for a given

value of the primary rotational degree of freedom of the notch [5]. This work presents a trial to overcome this situation by investigating different notch shapes with the objective of determining the shape of the transition between the bulk material and the hinge ('fillet' region) that allows the stress in the hinge to be minimised. Results obtained by comparing the stress-strain behaviour of the two limit cases (leaf spring (prismatic beam) shaped notches and circular hinges) with intermediate shapes based on optimised circular and elliptical fillet shapes, as well as on shapes obtained in classical mechanics via stress concentration minimisation criteria for shoulder fillets [7-9], are thus presented.

## 2. Hinge Shape Definitions

In order to allow the comparison of the different fillet shapes, for all the considered notches a constant hinge aspect ratio  $L/h_{\min}$  (Fig. 1) was assumed:

$$\gamma = \frac{L}{h_{\min}} = 25 \quad (1)$$

Such a value was chosen with the aim of emphasizing the effects of the fillet region, while concurrently meeting the technological limits imposed by today's precision manufacturing processes such as EDM, water jet cutting, laser cutting or deep X-ray lithography (experimental tests have, for example, shown that it is not possible to manufacture prismatic beams with aspect ratios greater than  $\gamma \sim 50$  without degrading significantly the machined surface quality [10]).

The other geometrical parameters of the considered flexural hinge shapes are shown in Fig. 2, where the zones A (fillet junction with bulk material), B (junction between fillet and prismatic segment) and C (hinge centre) define the expected maximum stress level regions.

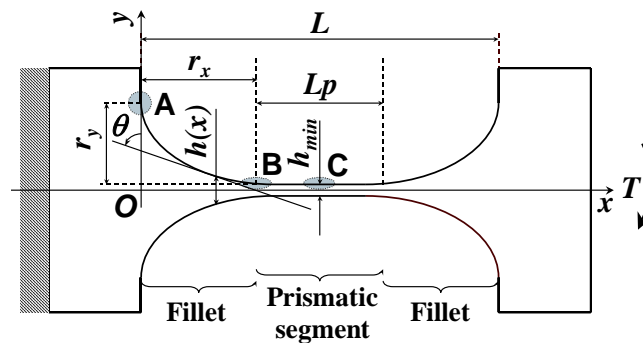


Fig. 1: Geometrical parameters used to define the hinge shapes under study:  $L$  – total length of the hinge,  $L_p$  – length of the prismatic segment of the hinge,  $h_{\min}$  – minimal thickness of the hinge,  $r_x$  and  $r_y$  – fillet length and height

Six different hinge shapes have been considered:

1. The prismatic beam hinge (leaf spring).
2. The circular hinge (conventional rotational joint). When  $r_x = L/2$  the hinge is designated as a 'right circular hinge'. In this study is considered the general case where a prismatic segment of length  $L_p$  can also be inserted between the two fillets (Fig. 2); this circular hinge shape has thus a free parameter  $r_x = r_y = r$  (coupled with  $L_p$ ) that could be optimised (see below):

$$0 < r \leq \frac{L}{2} \quad (2)$$

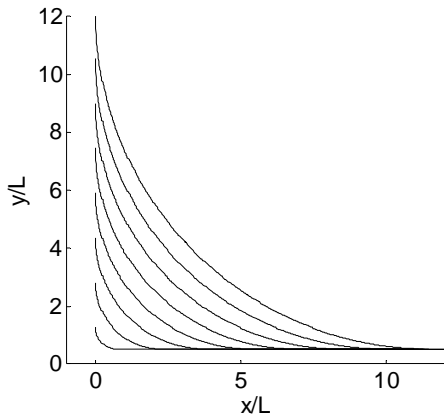


Fig. 2: The circular hinge family of shapes

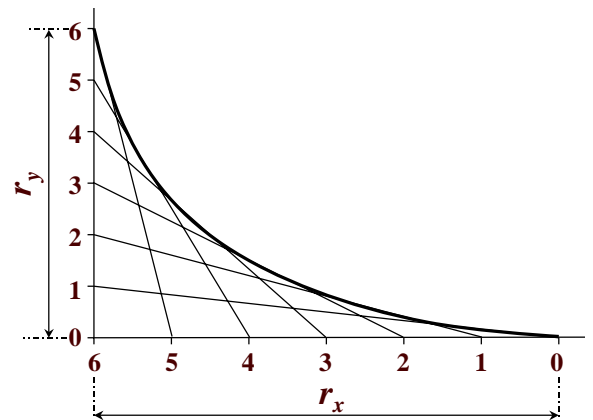


Fig. 3: The Grodzinski fillet shape

Given their broad usage in high-precision applications, the prismatic beam (leaf spring) and the circular hinge shapes will be used as the two limit cases to be compared with the other ('non-conventional') shapes.

3. Elliptical hinge: a variant of the circular hinge, where the segment of a circle is replaced with the segment of an ellipse whose semi-axes are  $r_x$  and  $r_y$ . The elliptical hinge has two free parameters that can be optimised (see below): the length of the prismatic section of the hinge  $L_p$  and the fillet aspect ratio  $r_y/r_x$ .
4. Grodzinski hinge [7] (Fig. 3 and 5): a hinge with fillets of parabolic shape. As shown in Fig. 3, the entities  $r_x$  and  $r_y$  are divided here into equal number of parts, but numbered in a reverse order; homonymous numbers are then connected enveloping a parabola. As in the case of the elliptical hinge, the Grodzinski fillet has two free parameters:  $L_p$  and  $r_y/r_x$ . In this case, however, as a first step, these parameters were assumed to be of a determined fixed value (see Table 2).
5. Baud hinge [8] (Fig. 4 and 5): the fillet shape has here the same contour as that given mathematically for an ideal, frictionless liquid freely flowing out from an opening at the bottom of a tank. The shape is thus determined from the well know fluid-dynamic similarity principles often applied to determine the effects of stress concentrators [11], and is thus called of 'streamline form'. This streamline curve, shown experimentally to produce practically no stress concentrations for a shoulder loaded in tension, has the fillet height of  $r_y = h_{\min}/\pi$  and is defined by the following parametric equations:

$$x = \frac{h_{\min}}{\pi} \left[ \ln \tan \left( \frac{\theta}{2} + \frac{\pi}{4} \right) - \sin \theta \right] \quad (3)$$

$$y = h_{\min} \left[ \frac{1}{2} + \frac{1}{\pi} \left( 1 - 2 \sin^2 \frac{\theta}{2} \right) \right] \quad (4)$$

$$0 \leq \theta \leq \pi/2 \quad (5)$$

The boundary conditions are given as:

- for  $\theta = 0$  ( $\theta$  is the inclination of the tangent to the fillet with respect to the y coordinate - Fig. 1):  
 $x = 0$  and  $y = h_{\min}(1/2 + 1/\pi)$
- for  $\theta = \pi/2$ :  $x \rightarrow \infty$  and  $y = h_{\min}/2$ .

The fillet length  $r_x$  would thus be infinite; by the assumption defined in eq. (1) it is, however, practically truncated to the desired aspect ratio, i.e.

$$r_x = \frac{\gamma h_{\min}}{2} \quad (6)$$

6. Thum & Bautz hinge: the Baud streamline fillet has been here optimised empirically for the bending case for which the material in the Baud fillet was not optimally used [8, 9]. The shape of this fillet is given in Table 1. Four such fillets joined so that the hinge aspect ratio value  $\gamma$  is maintained equal to 25 form then the Thum and Bautz hinge (Fig. 4 and 5).

Table 1: Geometrical parameters defining the Thum & Bautz fillet

$x/h_{\min}$	$h(x)/h_{\min}$	$x/h_{\min}$	$h(x)/h_{\min}$
0	1.475	0.3	1.052
0.002	1.420	0.4	1.035
0.005	1.377	0.5	1.026
0.01	1.336	0.6	1.021
0.02	1.287	0.7	1.018
0.04	1.230	0.8	1.015
0.06	1.193	0.9	1.012
0.08	1.166	1	1.010
0.1	1.145	1.3	1.005
0.15	1.107	1.6	1.003
0.2	1.082	$\infty$	1

The comparison of the geometrical parameters of the considered hinge shapes is given in Table 2, while the graphs of Fig. 4 and 5 allow their geometries to be compared.

Table 2: Geometrical parameters defining the considered hinge shapes

	prismatic beam	circular hinge	elliptical hinge	Grodzinski hinge [7]	Baud hinge [8]	Thum & Bautz hinge [9]
Fillets	no fillets (sharp right angle)	quarter of a circle of radius $r$	quarter of an ellipse ( $r_x$ and $r_y$ as semi-axes)	parabolas as on Fig. 3 with $r_x = r_y = h_{\min}$	parametric eq. (3), (4) and (5)	Table 1
$L/h_{\min}$	$L/h_{\min} = 25$	$L/h_{\min} = 25$	$L/h_{\min} = 25$	$L/h_{\min} = 25$	$L/h_{\min} = 25$	$L/h_{\min} = 25$
$L_p$	$L_p = L$	$L_p = L - 2r$	$L_p = L - 2r_x$	$L_p = L - 2r_x$	$L_p = 0$ ( $r_x = L/2$ )	$L_p = 0$ ( $r_x = L/2$ )
$r_y/r_x$	not defined	$r_y/r_x = 1$	free parameter	$r_y/r_x = 1$	$r_y/r_x = 0.0255$	$r_y/r_x = 0.019$

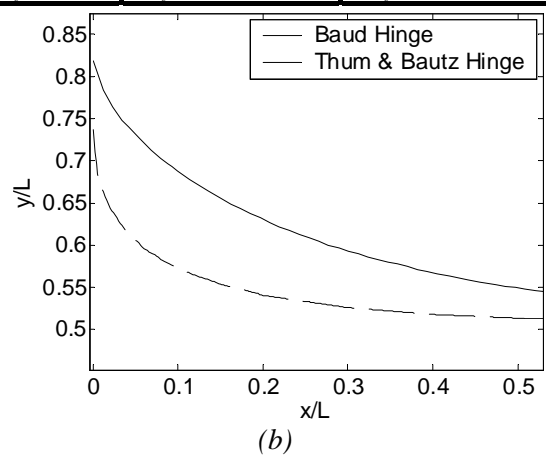
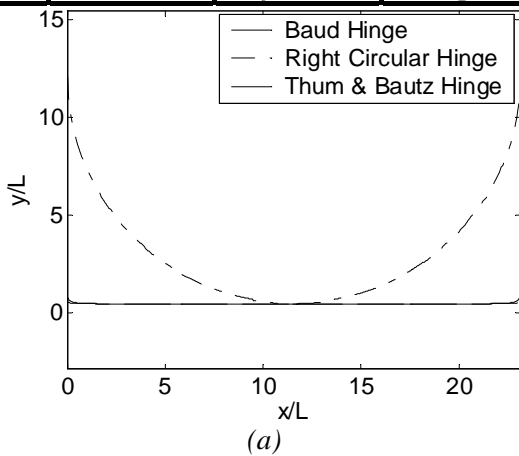


Fig. 4: Right circular, Baud and Thum & Bautz hinge shapes. The same scales are used for the  $x$  and  $y$  axes to show true proportions (a); an enlargement of the same graph (b) emphasises the difference between the Baud and the Thum & Bautz fillets

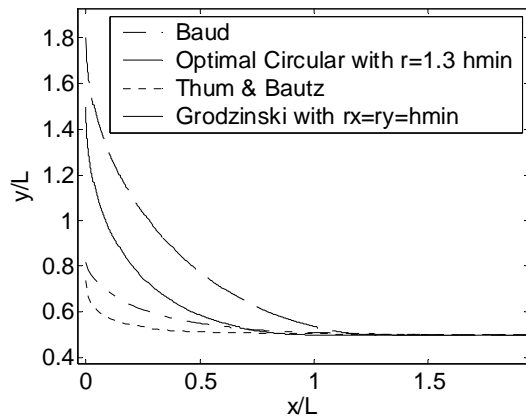


Fig. 5: Comparison of the circular ( $r = 1.3 h_{min}$ ), Grodzinski ( $r_x = r_y = h_{min}$ ), Baud and Thum & Bautz hinges

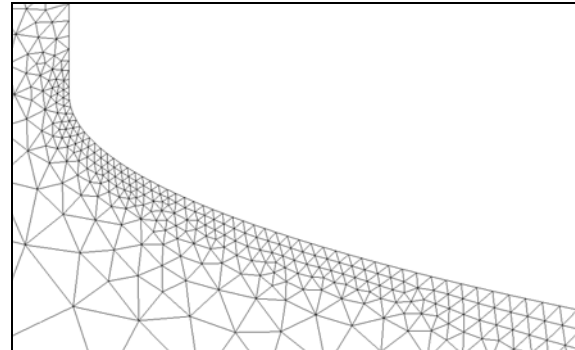


Fig. 6: Detail of the mesh used for the FEM simulation of an elliptical hinge

In Fig. 4 and 5 can be seen that the Grodzinski, Baud and Thum & Bautz shapes have a propensity towards a slender (prismatic beam) rather than a circular hinge. These hinges are therefore expected to be in any case more compliant than the circular one, allowing thus the stress in the hinge for a given deflection to be reduced. It should be mentioned, however, that these fillet shapes have been developed for bulky shoulder fillets, i.e. for axial-symmetric geometries [12]. On the other hand, the hinges considered in this work are planar (sheet) structures. However, the results reported in [11, 12] allow establishing that for the same load cases the stress behaviour in the two cases is very similar (for axial-symmetric cases the stress concentration factor is only slightly lower than that of planar geometries). Moreover, since here are considered reasonably thin structures, their behaviour can certainly be considered equivalent to that of the central portion of the axial-symmetric case, i.e. the possible influence of the boundary layer of the axial-symmetric case in the transversal direction can be neglected. Based on all these motivations, an investigation of the fillet shapes given in [7-9] seems a reasonable approach.

### 3. Hinge Shape Optimisation

The objective function for the optimisation is defined as the quest for a hinge that is subjected to the lowest stress for a given bending angle. Since the entity of the stress varies along the hinge length, the stress that will be considered is then the absolute maximum stress along the hinge, i.e. the stress that is likely to cause the hinge fatigue failure.

#### 3.1. Hinge Stress Calculation Methods

In all the performed calculations the hinges are rigidly fixed at one end and loaded with a pure bending torque  $T$  on the free end. The analytical calculation is then performed assuming that the hinges are beams of varying cross section, with  $b$  being the constant hinge width and  $h(x)$  being the hinge thickness varying along its length. The stress is thus calculated as:

$$\sigma(x) = \frac{6T}{bh^2(x)} \quad (7)$$

whereas the normalized stress in the hinge, expressed in  $\text{rad}^{-1}$  and independent of the hinge width  $b$ , is

$$\sigma_n = \frac{\sigma}{E\alpha} \quad (8)$$

The curvature formula of the hinge is

$$y''(x) = \frac{T}{EI(x)} \text{ where } I(x) = \frac{bh^3(x)}{12} \quad (9)$$

Here  $y''(x)$  is the second derivative of the deformed shape of the hinge and  $E$  is the Young's modulus of the used material.

The hinge angular stiffness is defined as

$$k_\theta = \frac{T}{y'(L)} = \frac{T}{\alpha} \quad (10)$$

where  $y'(L) = \alpha$ , used already in eq. (8), is the rotation angle of the tip of the hinge.

For a given rotation angle  $\alpha$ , these equations allow the corresponding bending torque  $T$  to be derived, as well as the maximum stress across the hinge to be calculated. In pure bending, the maximum stress will always occur where the thickness  $h(x)$  is minimal.

This analytical approach based on the classical structural mechanics gives accurate results if the beam cross-section varies slowly along the beam length. In the case of sharper variations of the cross section, stress concentration effects that are not taken into account appear as well. In the latter case, a Finite Element Method (FEM) approach is generally the preferred one. In the course of the work, FEM simulations were thus also performed for some of the hinges. Both the NASTRAN and the FEDEM FEM codes were used to ensure the correctness of the simulations. This has allowed the stress concentrations in the areas of sharply changing curvature (indeed the fillets) to be accurately studied. Three and four node shell elements were used for the non-linear analysis; the mesh was made denser in areas of expected stress peaks (Fig. 6).

The FEM approach has, however, proven to be more programming-time intensive than the analytical one. The two outlined approaches were hence used complementarily throughout the presented study.

### 3.2. Stress in the Prismatic Beam Hinge

The stress in the prismatic beam hinge that has perfectly sharp right angles at its ends (leaf spring) cannot be calculated by FEM, since a finite fillet radius would be required to estimate the stress concentration effects. As already pointed out, the calculation of the nominal stress for this case (no stress concentration) is, however, useful as a reference case for comparison with the other hinge shapes. The normalized stress calculated analytically for this case is thus

$$\sigma_{n\_prismatic}^{analytical} = \frac{h_{min}}{2L} = 0.0216 \text{ rad}^{-1}$$

For a leaf spring made of steel ( $E = 210$  GPa) whose free end is rotated by  $5^\circ$  (0.0873 rad) under a pure torque loading, the stress would thus be

$$\sigma = \sigma_{n\_prismatic} E \alpha = 0.0216 \cdot 210 \cdot 10^9 \cdot 0.0873 = 396 \text{ MPa.}$$

### 3.3. Stress in the Circular Hinge

In this case the fillet radius  $r$  is kept as a free parameter (Fig. 7). For  $r = L/2$  (right circular hinge) the normalized stress assumes the value of

$$\sigma_{n\_Right\_Circular}^{analytical} = 0.126 \text{ rad}^{-1}$$

which is 5.8 times bigger than for the prismatic beam hinge. As  $r$  is reduced (i.e. the length of the prismatic segment is increased), the compliance of the hinge increases thus reducing the normalized stress level. However, when  $r$  approaches  $h_{min}$ , stress concentration effects appear and a localized stress concentration at the junction between the prismatic segment and the fillet (zone B in Fig. 1) is observed. Hence, reducing  $r$  below a certain optimal value will cause the maximum stress level to rise. Using the FEM approach (Fig. 7 and 8) this optimal  $r$  value was established to be

$$r_{opt} = 1.3 \cdot h_{min} \quad (11)$$

while the corresponding normalized stress for this optimised circular hinge then turned out to be

$$\sigma_{n\_Circular}^{FEM} = 0.0254 \text{ rad}^{-1}$$

This value is 18% higher than that of the prismatic-beam hinge and still 5 times lower than that of the right circular hinge.

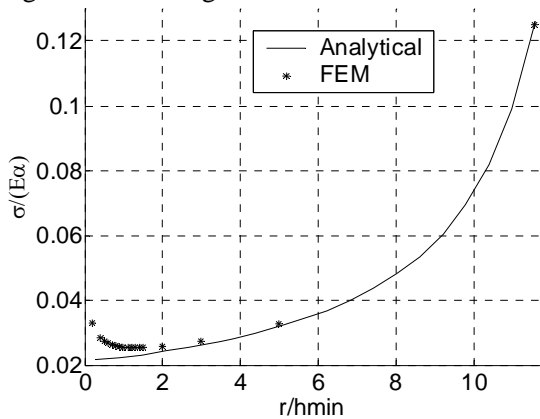


Fig. 7: Maximum normalized stress [ $\text{rad}^{-1}$ ] in the circular hinge. When  $r$  is reduced below  $2 \cdot h$  stress concentration effects (reflected by the FEM curve) appear

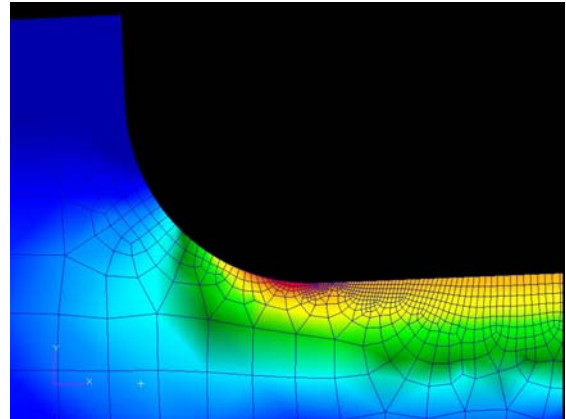


Fig. 8: Stress distribution in a circular hinge with fillet radius  $r_{opt} = 1.3 \cdot h_{min}$

### 3.4. Stress in the Elliptical Hinge

The particular case where  $L_p = 0$  corresponds to a ‘pure elliptical hinge’ without a prismatic segment (Fig. 9). The parameter that was optimised in this case is the fillet aspect ratio  $r_y/r_x$ .

In this case two high stress level zones appear: one at the hinge centre where the thickness is minimal (zone C in Fig. 1) - designated here as ‘gross stress’, and one at the fillet start where the radius of curvature can be sharp (zone A in Fig. 1) - designated here as ‘local stress’ (Fig. 10 and 11). As  $r_y/r_x$  is reduced, the gross stress decreases and the local stress increases. The optimal fillet aspect ratio corresponds then to the  $r_y/r_x$  value where the curves of the local and the gross stress intersect (Fig. 10), i.e.  $r_y/r_x = 0.022$ . In the considered case ( $L_p = 0$ ) this corresponds thus to

$$r_x = L/2, \quad r_y^{opt} = 0.011 \cdot L \quad (12)$$

The normalized stress level of this optimised pure elliptical hinge is then

$$\sigma_{n\_Pure\_elliptical}^{opt} = 0.0275 \text{ rad}^{-1}$$

i.e. 8% higher than by the optimised circular hinge, 27% higher than in the leaf spring case but still 4.6 times lower than by the right circular hinge.

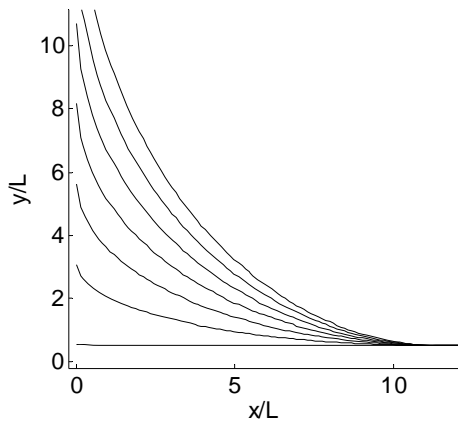


Fig. 9: The pure elliptical hinge family

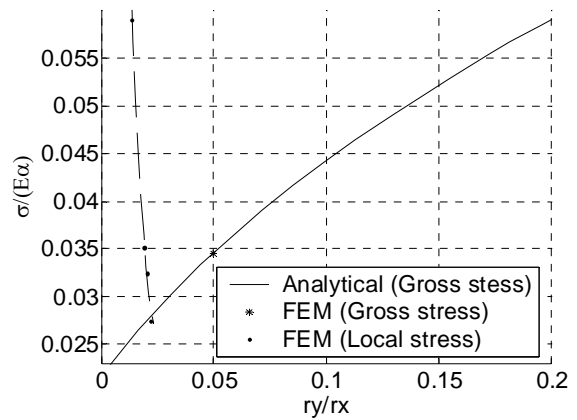


Fig. 10: Maximum normalized stress [ $\text{rad}^{-1}$ ] in the pure elliptical hinge

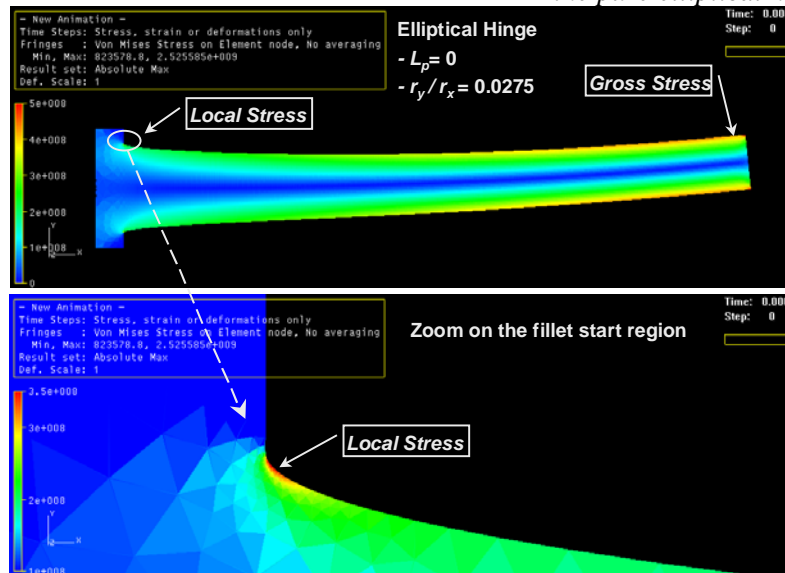


Fig. 11: Stress distribution along the elliptical hinge. The upper picture shows one half of the hinge, the lower one is giving an enlargement of the 'local stress' critical zone

In the particular case of elliptical hinges where  $r_y$  is chosen to be equal to that of the Baud hinge ( $r_y = h_{\min}/\pi$ ), the  $r_x$  semi-axis of the ellipse (that is coupled to the prismatic segment length through  $L_p = L - 2 \cdot r_x$ ) is the free parameter to be optimised (Fig. 12 and 13). In this case  $r_y/r_x = 0.21$  was obtained as the optimal value (Fig. 13), so that

$$r_x^{opt} = 0.061 \cdot L, \quad r_y = r_{y\_Baud} = 0.0127 \cdot L, \quad L_p^{opt} = 0.878 \cdot L \quad (13)$$

and the respective normalized stress level is

$$\sigma_{n\_Elliptical}^{opt} = 0.023 \text{ rad}^{-1}$$

This value is only 6.5% higher than that of the prismatic beam and meaningfully lower than the normalized stresses in the optimised circular and optimised pure elliptical hinge.

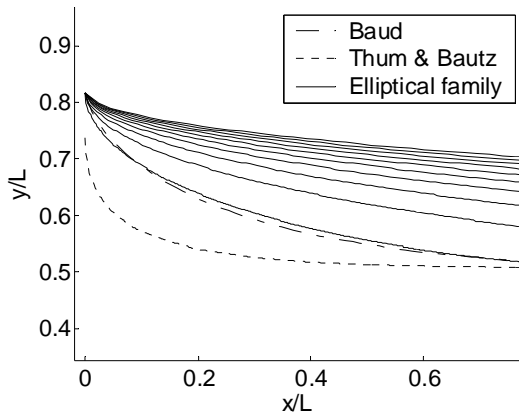


Fig. 12: Elliptical hinges with  $r_y = r_{y\_Baud}$  - for comparison are shown also the Baud and the Thum & Bautz shapes

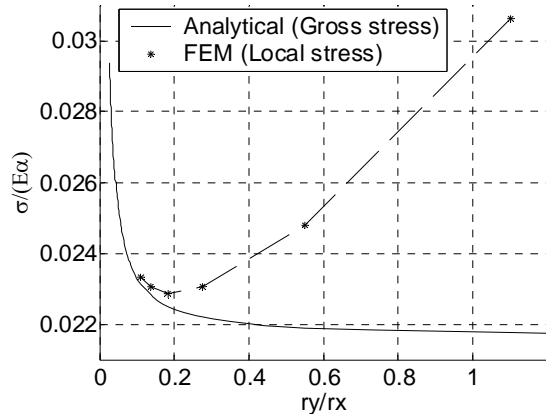


Fig. 13: Maximum normalized stress [ $\text{rad}^{-1}$ ] in the elliptical hinge with  $r_y = h_{\text{min}}/\pi$ . For  $r_y/r_x$  values greater than 0.1 stress concentration effects appear

### 3.5. Stress in the Grodzinski Hinge

The normalized stress in the Grodzinski hinge calculated with the analytical method is

$$\sigma_{n\_Grodzinski}^{\text{analytical}} = 0.0224 \text{ rad}^{-1}$$

A FEM simulation (Fig. 14) of this shape showed a stress concentration factor of 1.1 at the location of zone B in Fig. 1. The maximum normalized stress is thus

$$\sigma_{n\_Grodzinski}^{\text{FEM}} = 1.1 \cdot \sigma_{n\_Grodzinski}^{\text{analytical}} = 0.0245 \text{ rad}^{-1}$$

This value is hence within 4% from that of the optimised circular hinge, which is also understandable observing in Fig. 5 that the two shapes are similar.

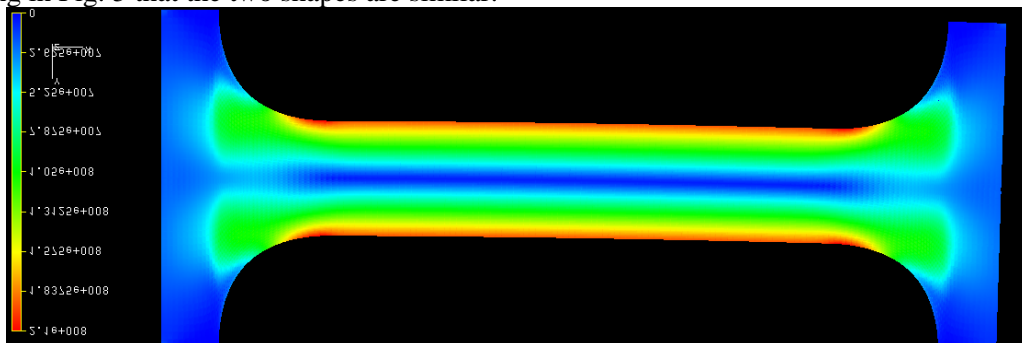


Fig. 14: Stress distribution in a prismatic hinge with Grodzinski fillets; the stress level at the junction between the fillets and the prismatic segment is slightly higher than that in the hinge centre resulting in a stress concentration factor of 1.1

### 3.6. Stress in the Baud Hinge

In the case of the Baud hinge the maximum stress appears at the hinge centre (i.e.  $\sigma_{\max}(x) = \sigma(L/2)$  - zone C in Fig. 1). The normalized stress in the Baud hinge calculated with the analytical and the FEM approach is respectively

$$\sigma_{n\_Baud}^{analytical} = 0.0223 \text{ rad}^{-1} \quad \sigma_{n\_Baud}^{FEM} = 0.0216 \text{ rad}^{-1}$$

The difference between the two calculation methods is therefore 3%, with the analytical value being only 3% higher than that of the leaf spring (5.7 times higher than by the conventional right circular hinge). This justifies thus once more the need to consider the streamline fillet shapes developed for bulky axial-symmetric shoulders also in the case of planar structures.

### 3.7. Stress in the Thum & Bautz Hinge

The normalized stress in the Thum & Bautz hinge calculated with the analytical and the FEM method is

$$\sigma_{n\_TB}^{analytical} = 0.0219 \text{ rad}^{-1} \quad \sigma_{n\_TB}^{FEM} = 0.0228 \text{ rad}^{-1}$$

The analytical value is hence 1.8% lower than that of the Baud Hinge, 5% lower than that of the optimised elliptical hinge with  $r_y = r_{y\_Baud}$  (cf. in this regard Fig. 12), and merely 1.4% higher than that of the prismatic beam hinge where no stress concentrations are considered. In terms of stress levels, this shape presents thus very small improvement potential and, among the considered cases, the respective fillet can thus be considered to be the absolute optimum.

## 4. Parasitic Shift Calculation

In the case of the classical circular hinges the rotation axis is localized near their thinnest portion (in this point is then also concentrated the stress, which limits the reachable deflections). On the other hand, by employing a leaf spring the deflection is distributed over its length thus lowering the stresses, but the hinge point is not fixed and it moves along the beam as it deflects [5]. It literature was already shown that in the latter case (e.g. by using flexural pivots [13]), the overall precision of the positioning devices can thus be considerably decreased. The parasitic deflections of the considered hinge shapes have therefore been evaluated analytically and numerically, allowing hence preliminary guidelines for the designers of high-precision mechanisms based on flexural hinges to be provided.

### 4.1. Parasitic Shift Calculation Methods

A joint with a pure rotational degree of freedom is considered (Fig. 15). Its in-plane imperfections are taken into account by following the motion of a point P' linked to the mobile block, which, at the start of the movement, is superimposed with point P - the ideal centre of rotation of the joint. In case of a perfect joint, after the rotation of the mobile block by an angle  $\alpha$ , point P' would remain superimposed with P; if, however, the joint has in-plane rotational imperfections, P' is shifted away. The vector **PP'** is then designated as 'parasitic shift'.

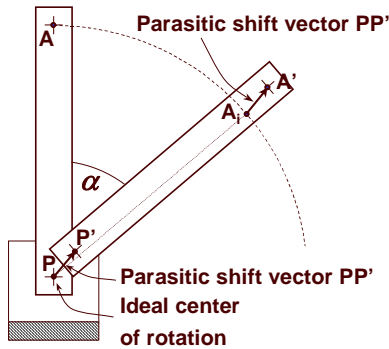


Fig. 15: Parasitic shift concept

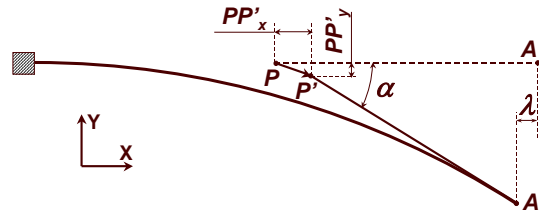


Fig. 16: Parasitic shift of flexural hinges: after rotating the hinge by an angle  $\alpha$ , segment PA moves to P'A'

Once  $\mathbf{PP}'$  is known, the calculation of the position of other points of the mobile block is straightforward: point A moves to A', which corresponds to the ideal position of A (which would have been reached if the joint was perfect) translated by the parasitic shift vector  $\mathbf{PP}'$ .

In the case of necked down (slender) flexural hinges, the ideal centre of rotation is the centre of symmetry of the joint (Fig. 16). The magnitude of the parasitic shift  $\mathbf{PP}'$  is here

$$PP' = \sqrt{PP'_x{}^2 + PP'_y{}^2} \quad (14)$$

The x and y coordinates of the free end of the hinge are

$$A'_x = A_x - \lambda \quad \text{and} \quad A'_y = y(L) \quad (15)$$

where the well-known expression for the axial deformation  $\lambda$  of the hinge, calculated considering the variation of its length from the initially straight form to the deformed shape in the equilibrium condition [14], is used:

$$\lambda = \frac{1}{2} \int_0^L (y'(x))^2 dx \quad (16)$$

whereas the terms  $y'(x)$  and  $y(L)$  are calculated with the usual approximated expression of beam curvature in which the square of the derivative is neglected [13]. Once  $A'_x$ ,  $A'_y$  and  $\alpha$  are known, the position of P', and thus the parasitic shift vector, can be derived from geometrical considerations.

To validate this approximated analytical approach, FEM parasitic shift calculations were used to study the deviation of some of the hinges from an ideal pivot kinematics. This effect is non-linear of nature and it turned out to be rather difficult to obtain good results using shell finite elements. In fact, by using non-linear analysis in NASTRAN, the sensitivity of the simulations, as well as the 'microscopic' nature of the parasitic effect, gave poor results. Beam elements were thus used and gave better results. These required, however, an extensive work to define the varying cross-section properties. Only a few hinges were thus analysed with the FEM approach.

#### 4.2. Parasitic Shift of the Prismatic Beam Hinge

To verify the proposed approximated analytical parasitic shift calculation method, the results obtained by its application have been used first for the calculation of the well-established prismatic beam hinge case.

From the exact curvature formula it is obvious that the deformed shape of the prismatic beam hinge is a segment of a circle. It is thus possible to calculate geometrically the x and y components of the parasitic shift vector as

$$PP'_x = L \cdot \left( \frac{\sin \alpha}{\alpha} - \frac{\cos \alpha + 1}{2} \right)$$

$$PP'_y = L \cdot \left( \frac{\cos \alpha - 1}{\alpha} + \frac{\sin \alpha}{2} \right)$$
(17)

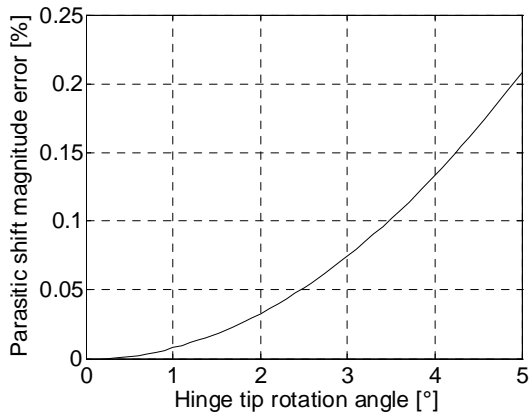


Fig. 17: Difference between the magnitude of the parasitic shift calculated with the exact and the approximated analytical methods

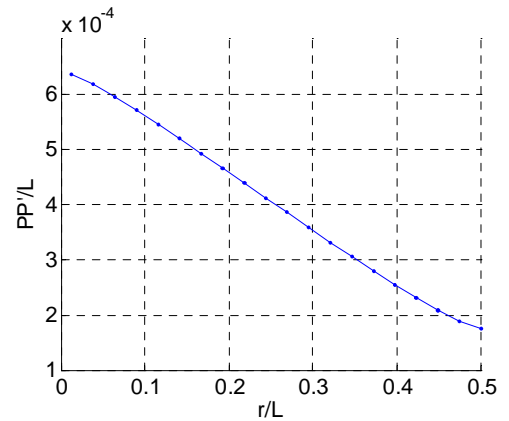


Fig. 18: Parasitic shift magnitude of the circular hinge with respect to the normalized fillet radius  $r/L$  for a  $\alpha = 5^\circ$  rotation

A comparison of this exact parasitic shift value with the value obtained via the approximate analytical method described above is given in Fig. 17. It can thus be seen that for small rotations the simplified analytical method gives accurate results; as the rotation angle is increased, the error increases exponentially. Nevertheless, if the angle is kept reasonably small ( $< 5^\circ$ , i.e. in the region where the influence of the geometrical non-linearities is still limited [13]) the error on the magnitude remains smaller than 0.21%. On the other hand, FEM simulated non-linear behaviour of the prismatic-beam hinge for a rotation  $\alpha = 5^\circ$  allowed obtaining a value of the parasitic shift vector magnitude of

$$PP'_{prismatic}{}^{FEM} = 6.340 \cdot 10^{-4} \cdot L$$
(18)

In Table 3 is given the comparison of the results of the normalised parasitic shift magnitude  $PP'/L$  obtained with the exact and the approximated analytical approach, as well as via a FEM approach, validating thus the approximated analytical method in the case of the prismatic beam hinge. This method has therefore been used to calculate also the magnitude of the parasitic shifts of the other considered hinge shapes.

Table 3: Comparison of the parasitic shift results for the prismatic beam hinge

Calculation method	Normalized parasitic shift magnitude for a rotation angle $\alpha = 5^\circ$	Error with respect to 'exact' value
Exact analytical formulation	$PP'_{prismatic}{}^{exact} / L = 6.345 \cdot 10^{-4}$	/
Approximated analytical approach	$PP'_{prismatic}{}^{approx} / L = 6.358 \cdot 10^{-4}$	0.2%
FEM	$PP'_{prismatic}{}^{FEM} / L = 6.340 \cdot 10^{-4}$	-0.08%

### 4.3. Parasitic Shift of the Circular Hinges

The leaf spring hinge is a particular case of a circular hinge with  $r = 0$  for which the normalised parasitic shift is  $6.358 \cdot 10^{-4}$  (approximated analytical method result for a  $5^\circ$  rotation). The right circular

hinge is another particular case of the circular hinge with  $r/L = 0.5$ ; in this case the normalized parasitic shift for a  $5^\circ$  rotation is

$$PP_{Right\_circular}^{analytical} / L = 1.748 \cdot 10^{-4}$$

i.e. 3.6 times smaller than for the prismatic beam hinge.

As shown in Fig. 18, between these two extreme cases the normalized parasitic shift varies almost linearly with respect to  $r$ . A calculation of the normalized parasitic shift of the right circular hinge for a  $5^\circ$  rotation was performed also via non-linear FEM analysis:

$$PP_{Right\_circular}^{FEM} / L = 1.675 \cdot 10^{-4}$$

This value is 4% higher than the corresponding analytical result.

In section 3.3. was shown that there is an optimised circular hinge with fillet radius  $r_{opt} = 1.3 \cdot h_{min}$  that is subjected to the least stress for a given rotation angle. For a given hinge aspect ratio  $\gamma = 25$  this gives  $r_{opt}/L = 0.052$ . The corresponding parasitic shift (Fig. 18) is then

$$PP_{Circular}^{analytical} / L = 6.014 \cdot 10^{-4}$$

which is still 3.4 times bigger than for the conventional circular hinge, but also 9% smaller than for the leaf spring.

#### 4.4. Parasitic Shift of the Elliptical Hinges

Fig. 19 shows the parasitic shift of the pure elliptical hinge. Interesting particular cases are  $r_y/r_x \rightarrow 0$  (corresponding to the prismatic beam hinge),  $r_y/r_x = 1$  (corresponding to the right circular hinge) and  $r_y/r_x = 0.022$  (corresponding to the optimised pure elliptical hinge of section 3.4.). The normalized parasitic shift in the latter case is

$$PP_{Pure\_elliptical}^{analytical} / L = 5.58 \cdot 10^{-4}$$

i.e. 7% smaller than for the optimised circular hinge, 12% smaller than for the prismatic beam hinge and 3.2 times bigger than for the right circular hinge.

In Fig. 20 are shown the parasitic shifts of the elliptical hinges that have the same fillet height  $r_y$  as the Baud hinge. As shown above, the optimal hinge of this family has a fillet ratio  $r_y/r_x = 0.21$  so that the corresponding normalized parasitic shift magnitude in this case equals

$$PP_{Elliptical}^{analytical} / L = 6.21 \cdot 10^{-4}$$

This value is 3% higher than that of the optimised circular hinge, 11% higher than that of the optimised pure elliptical hinge, merely 2% lower than the parasitic shift magnitude of the leaf spring and 3.6 times higher than that of the right circular hinge.

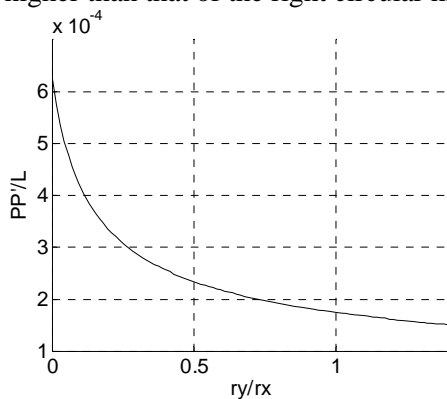


Fig. 19: Normalized parasitic shift of the pure elliptical hinge for a  $\alpha = 5^\circ$  rotation

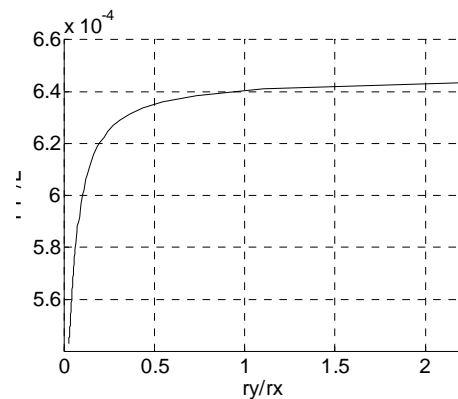


Fig. 20: Normalized parasitic shift of the elliptical hinge with  $r_y = r_{y\_Baud}$  for a  $\alpha = 5^\circ$  rotation

#### 4.5. Parasitic Shift of the Grodzinski, Baud and Thum & Bautz Hinges

According to the approximated analytical approach, the normalized parasitic shift magnitude of the Grodzinski hinge for a  $5^\circ$  rotation is

$$PP_{Grodzinski}^{analytical} / L = 6.14 \cdot 10^{-4}$$

For the same rotation, the normalized parasitic shift of the Baud hinge is

$$PP_{Baud}^{analytical} / L = 6.2 \cdot 10^{-4}$$

while the normalized parasitic shift of the Thum & Bautz hinge is

$$PP_{TB}^{analytical} / L = 6.3 \cdot 10^{-4}$$

These values are hence very close to that of the optimised elliptical hinge with  $r_y = r_{y\_Baud}$  (the differences being respectively -1%, 0.2% and 1%). Their ratios to the parasitic shift values obtained for the right circular hinge, the optimised circular hinge, the optimised pure elliptical hinge and the prismatic beam hinge are therefore correspondingly close to those cited above for the optimised elliptical hinge which has the same fillet height  $r_y$  as the Baud hinge.

## 5. Comparison Between Hinges

### 5.1. Normalized Stresses

A comparison of the normalized stresses of the studied hinges given in Fig. 21 evidences the fact that the Baud and the Thum & Bautz hinge shapes have stress levels that are very close to an idealized prismatic beam that has no stress concentration (with the Thum & Bautz shape being subjected to slightly lower stresses than the Baud hinge). In terms of stresses, these shapes present thus very little room for further improvements, and are indeed better than the other analysed shapes. In fact, the optimised elliptical hinge that has the same fillet height  $r_y$  as the Baud hinge is subjected to 3% more stress than the latter for the same bending angle. The optimised pure elliptical hinge, the optimised circular hinge and the Grodzinski (parabolic fillet) hinge are respectively subjected to 26, 16 and 12% more stress than the Thum & Bautz hinge. All these shapes are, however, far more compliant than the conventional right circular hinge, which is subjected to as much as 5.75 times higher normalized stresses than the Thum & Bautz hinge.

### 5.2. Parasitic Shift Magnitude for a $5^\circ$ Rotation

As shown on Fig. 21, the price to pay for the increased compliance of the hinges is the resulting parasitic shift. It is in fact clear that all the slender shapes approaching the leaf spring have parasitic shifts magnitudes that for a  $5^\circ$  rotation are between 3.6 (Thum & Bautz) and 3.2 (optimised pure elliptical hinge) times higher than that of the right circular hinge. The Thum & Bautz hinge, the optimised elliptical hinge with  $r_y = r_{y\_Baud}$ , the Baud hinge, and the Grodzinski hinge (in this particular order) are then the hinges which, in terms of the parasitic shift magnitude, come the closest (between 1 and 3.6%) to the idealised prismatic beam hinge. On the other hand, the optimised circular and pure elliptical hinges produce respectively 13 and 5% smaller parasitic shifts than the Thum & Bautz hinge.

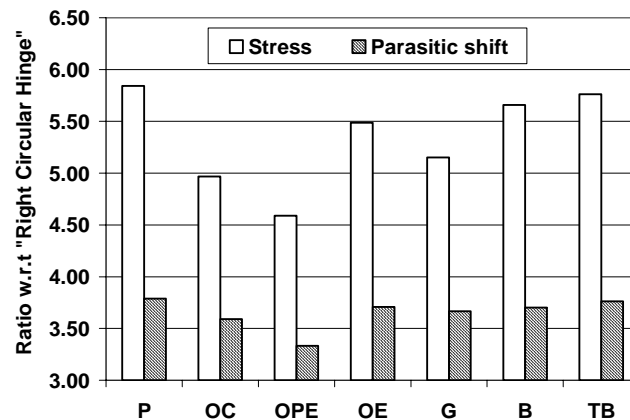


Fig. 21: Ratio of the normalized stress of the right circular (RC) hinge vs. the normalized stress of the other hinges (white bars) and ratio of the parasitic shift of the various hinges vs. the parasitic shift of the RC hinge (hachured bars). *P* - prismatic beam hinge, *OC* - optimised circular hinge, *OPE* - optimised pure elliptical hinge ( $L_p = 0$ ), *OE* - optimised elliptical hinge with  $r_y = r_{y\_Baud}$  *G* - Grodzinski hinge, *B* - Baud hinge, *TB* - Thum & Bautz hinge

The choice of the optimal hinge shape for a particular application will thus necessarily depend on a trade-off between compliance and parasitic shift.

## 6. Conclusions and Outlook

This work presents a first systematic attempt towards the optimisation of the shape of flexural hinges to be used in the design of high-precision positioning mechanisms for synchrotron radiation and other instrumentation. It is shown that by optimising the shape of the conventional circular hinges, as well as by adopting optimised elliptical or shapes obtained originally via stress concentration minimisation criteria for bulky shoulder fillets, a considerable increase of the compliance of the notches can be obtained. This results in far lower stresses for a given rotation angle or, alternatively, in a far larger displacement range before reaching the fatigue lifetime limit; the considered streamline fillet shapes present, in fact, very little room for further improvement with respect to an idealised case of a prismatic beam with no stress concentration. This in turn confirms also the validity of the assumption that the stress-strain behaviour of planar geometries can be considered equivalent to that of the central portion of axial-symmetric shoulder fillets.

The compliance increase can, however, be achieved only at the expense of an increase of the parasitic shift. The designer, depending on the particular application, will thus be able to choose a configuration such as the Thum & Bautz or Baud shape, if he is concerned mainly with stress minimisation, or alternatively the optimised circular or pure elliptical shapes, if he will be aiming at a parasitic shift minimisation while still wishing smaller stresses than those of a conventional right circular hinge.

The here obtained results are limited to a fixed hinge aspect ratio value of 25. A preliminary investigation of the influence of the aspect ratio on the stress and parasitic shift values has allowed establishing that the normalised stress is inversely proportional to the hinge aspect ratio  $L/h_{\min}$ . The improvement of the compliance with the increase of the hinge aspect ratio is, however, less pronounced in the case of the pure elliptical hinge and the right circular hinge; in the latter case the compliance is, in fact, increasing proportionally to the square root of the aspect ratio. It is important to mention here also that the optimised hinge dimensions are valid only for a specific value of the hinge aspect ratio and would have to be established again for other aspect ratios.

For slender hinges (those tending to the prismatic beam shape) the normalised parasitic shift seems to be roughly independent on the hinge aspect ratio. In the case of the conventional right circular hinge, the normalised parasitic shift decreases as  $L/h_{\min}$  is increased (Fig. 22). Intuitively can this be explained

by the fact that for a hinge of a constant length whose minimal thickness  $h_{\min}$  is reduced the compliance will tend to become clustered in the centre of the hinge, i.e. the portions of the hinge being further away from its centre will contribute less to the total rotation. A similar phenomenon is taking place also for the pure elliptical hinge.

Increasing the hinge aspect ratio  $L/h_{\min}$  would thus seem to constitute an appropriate solution since such a scheme increases the compliance of the hinge while concurrently, in the worse case, not affecting the normalised parasitic shift magnitude (this, however, means that for a constant  $h_{\min}$  and an increasing  $L$ , the absolute value of the parasitic shift would still grow).

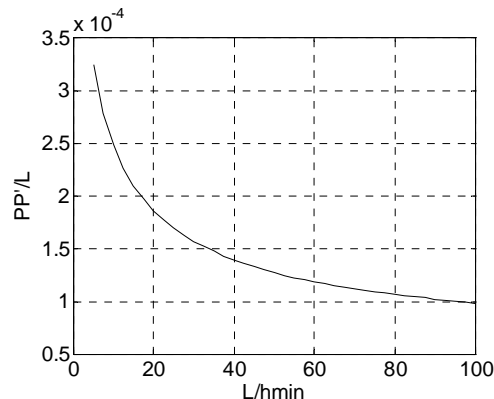


Fig. 22: Normalized parasitic shift magnitude of the right circular hinge vs. its aspect ratio

To validate experimentally all of the above theoretical result, an extensive fatigue test campaign on EDM produced hinges is planned in the near future.

## References

- [1] S. Zelenika, "Mechanical Aspects of the Design of 3<sup>rd</sup> Generation Synchrotron Light Sources", CERN Accelerator School Proc., to be published.
- [2] S. Henein, I. Kjelberg, S. Zelenika, "Flexible Bearings for High-Precision Mechanisms in Accelerator Facilities", Proc. NANOBEAM 2002, Lausanne (CH), 2002, pp. 103-110.
- [3] D. Shu, Th. S. Toellner, E. E. Alp, "Modular overconstrained weak-link mechanism for ultraprecision motion control", Nucl. Instr. Meth. Phys. Res. A467-468 (2001) 771-774.
- [4] T. Noll et al., "The Monolithic Two Axis Flexure Joined Mirror Support and the Mechanical Design of the Infrared Beamline", Proc. MEDSI 2002, Argonne (USA), 2002, pp. 65-73.
- [5] S. T. Smith et al., "Elliptical flexure hinges", Rev. Sci. Instr. 68 (3) (1997) 1474-1483.
- [6] N. Lobontiu et al., "Parabolic and hyperbolic flexure hinges: flexibility, motion precision and stress characterisation based on compliance close-form equations", Prec. Eng. 26 (2002) 183-192.
- [7] P. Grodzinski, "Investigation on shaft fillets", Engineering 152 (1941) 321-324.
- [8] R.V. Baud, "Beiträge zur Kenntnis der Spannungsverteilung in prismatischen und keilförmigen Kronstrukturelementen mit Querschnittübergängen", Ph. D. thesis, EHT Zürich, 1934.
- [9] A. Thum, W. Bautz, "Der Entlastungsübergang – Günstigste Ausbildung des Überganges an abgesetzten Wellen u. dgl.", Forschung Ingenieurwesen 6 (1934), 269-273.
- [10] S. Henein, "Conception des guidages flexibles", Press. Polytech. Uni. Romandes, Lausanne (CH), 2001.
- [11] A. Strozzi, "Costruzioni di macchine", Pitagora, Bologna (I), 1998.
- [12] R. E. Peterson, "Stress Concentration Design Factors", Wiley & Sons, New York (USA), 1953.
- [13] S. Zelenika, F. De Bona, "Analytical and Experimental Characterisation of High-Precision Flexural Pivots Subjected to Lateral Loads", Prec. Eng. 26(4) (2002) 381-388.
- [14] S. P. Timoshenko, J. M. Gere, "Theory of Elastic Stability - 2<sup>nd</sup> ed.", McGraw-Hill, New York, 1961.